

Deformations of Reinforced Concrete Members at Yielding and Ultimate

by Telemachos B. Panagiotakos and Michael N. Fardis

A database of more than 1000 tests (mainly cyclic) on specimens representative of various types of reinforced concrete (RC) members (beams, columns, and walls) is used to develop expressions for the deformations of RC members at yielding or failure (at ultimate), in terms of member geometric and mechanical characteristics. Expressions for the yield and the ultimate curvature based on the plane-section assumption provide good average agreement with test results, but with large scatter. The same applies to models for the ultimate drift or chord-rotation capacity based on curvatures and the concept of plastic hinge length. Semi-empirical models for the drift or chord-rotation at member yielding provide good average agreement with test results, but with considerable scatter. Their predictions and the associated test results point to effective secant stiffness at yielding around 20% of that of the uncracked gross section. An empirical expression is also developed for the ultimate drift or chord rotation in terms of: steel ductility; bar pull-out from the anchorage zone; load cycling; ratios of tension; compression; confinement or diagonal reinforcement; axial load ratio; $v = N/A_g f_c'$; shear-span ratio; and concrete strength. This expression is characterized by less scatter than alternatives with a more fundamental basis, and applies over a very wide range of parameter values for all types of RC members used in earthquake-resistant structures, including beams or columns with conventional or diagonal reinforcement and shear walls.

Keywords: deformation; ductility; stiffness; tests

INTRODUCTION

The inelastic deformation capacity of reinforced concrete (RC) members is important for the resistance of RC structures to imposed deformations, such as those due to settling of supports, temperature or shrinkage, and for moment redistribution under gravity loads. It is even more important for seismic loads because earthquake-resistant design relies on ductility, that is, on the ability of RC members to develop (cyclic) deformations well beyond elastic limits without significant loss of load-carrying capacity. Values of the force-reduction factor R of conventional force-based earthquake-resistant design depend on the deformation capacity of RC members, while detailing rules are specified for RC members so that they provide the required deformation capacity.

Due to the emergence of displacement-based concepts for seismic design of new structures and seismic evaluation of old ones, quantification of deformation capacity in terms of geometric and mechanical characteristics of members and of their reinforcement have attracted increased interest in recent years. The 1997 NEHRP Guidelines for the Seismic Rehabilitation of Buildings¹⁻³ base member evaluation on a capacity-demand comparison in terms of (member) deformations. These guidelines, known as FEMA 273/274^{1,2} and more recently FEMA 356,³ as well as other current procedures for the analysis of the seismic response of RC structures, require realistic values of the effective cracked

stiffness of RC members up to yielding for reliable estimation of the seismic force and deformation demands. If the elastic member stiffnesses used for the analysis effectively reproduce secant member stiffness to yielding, even a linear-elastic analysis with 5% damping can satisfactorily approximate inelastic seismic displacement and deformation demands.¹⁻⁴ To this end, tools are needed for the calculation of the secant stiffness to yielding for known geometric and mechanical characteristics of RC members.

The secant stiffness to yielding and the ultimate deformation of RC members are commonly determined (assuming purely flexural behavior) from section moment-curvature relations and integration thereof along the member length. Such a calculation does not commonly account for the effects of shear and inclined cracking, bond-slip phenomena, bar buckling, or even load cycling. More advanced models that incorporate the effects of inclined cracking, bond-slip, and tension stiffening, and account for the detailed σ - ϵ behavior of the reinforcement have also been proposed for the plastic rotation capacity of beams under monotonic loading.^{5,6} The primary motivation of those models was the quantification of the capacity for moment redistribution in connection with the bond and fracture properties of steel, especially in relation with some brittle cold-worked steels currently used in nonseismic or low seismicity regions of Europe. Despite their sophistication, these models have thus far not been very successful in effectively reproducing the experimental behavior up to ultimate.

Test results constitute the ultimate recourse for validation, calibration, or even development of models. This is particularly true for complex phenomena, such as the deformational behavior of concrete members up to failure in monotonic or cyclic loading. With this in mind, a large bank of experimental data was assembled and used herein for the development of simple models for the deformations of RC members at yielding and at failure. The primary deformation measure considered herein is the drift or chord rotation θ of a member over the shear span L_s . This measure captures the macroscopic behavior of the member as a whole, relates readily to more global measures of seismic response—such as story drifts—while at the same time suffices for signaling failure at the local level. Curvatures ϕ at yielding and ultimate are also considered, as potential intermediate steps for the determination of the corresponding values of θ for the entire member.

ACI Structural Journal, V. 98, No. 2, March-April 2001.

MS No. 99-199 received September 22, 1999, and reviewed under Institute publication policies. Copyright © 2001, American Concrete Institute. All rights reserved, including the making of copies unless permission is obtained from the copyright proprietors. Pertinent discussion will be published in the January-February 2002 *ACI Structural Journal* if received by September 1, 2001.

Telemachos B. Panagiotakos is a postdoctoral researcher in the Structures Laboratory at the University of Patras, Greece, where he received his Doctoral degree. His research interests are in earthquake resistance design of reinforced concrete structures.

ACI member Michael N. Fardis is Professor of Design of Concrete Structures at the University of Patras, Greece. He received the ACI Wason Medal in 1993.

Two approaches are pursued in this study: a statistical (or empirical) approach, as in References 7 and 8; and a more fundamental approach developed from basic principles and the mechanics of reinforced concrete.⁹⁻¹¹

RESEARCH SIGNIFICANCE

This study develops expressions for the ultimate deformation capacity and for the deformation at yielding of RC members, in terms of their geometric and mechanical characteristics. Such expressions are essential for the application of displacement-based procedures for earthquake-resistant design of new RC structures and for seismic evaluation of old ones. They are also essential for a realistic estimation of the effective elastic stiffness of cracked RC members and structures, which is important for the calculation of seismic force and deformation demands.

EXPERIMENTAL DATABASE

The database used in this study is comprised of 1012 tests of RC members in uniaxial bending, with or without axial force. The full characterization of test specimens and the experimental results, as well as the associated list of references, is given in the Appendix.* Out of these specimens, 266 can be considered as representative of beams because they have unsymmetric reinforcement and were tested under zero axial load (all specimens have rectangular cross section, with the exception of two, which have a T-section); 682 can be considered as column specimens with a symmetrically reinforced square or rectangular section, tested with or without axial force; 61 specimens are walls with a rectangular, barbelled, or T-section; and 23 of the column specimens have diagonal reinforcement, combined or not with conventional longitudinal bars.

Most specimens were of the simple or double cantilever type. In these specimens, some slippage of the longitudinal reinforcement from its anchorage beyond the section of maximum moment is possible in principle, contributing a fixed-end rotation to the overall drift of the specimen and increasing the average curvature measured next to the end. Many specimens were of the simply supported beam type, loaded with a force at midspan. Due to symmetry in these specimens, there was no slippage of the longitudinal reinforcement from an anchorage block at the section of maximum moment, except when the load was applied through a bulky stub at midspan, with enough dimension along the specimen axis for reinforcement slippage to develop on both sides of the midspan section.

In 296 tests, the relative rotation between the section of maximum moment and a nearby section within the plastic hinge region was measured and translated into an average curvature ϕ . In 124 of these tests, some slippage of the reinforcement from its anchorage beyond the section of maximum moment is, in principle, possible. In these in-

stances, curvatures include the effect of the associated fixed-end rotation.

In 963 specimens, deflections were measured in addition to or instead of curvatures, to be translated herein into drift θ , that is, deflection divided by distance from the section of maximum moment. If the deflection is measured at the point of zero moment, θ is equal to the chord rotation of the section of maximum moment. In 786 of these specimens, slip of reinforcement from its anchorage beyond the section of maximum moment was, in principle, possible.

With the exception of 35 of the tests where curvatures ϕ were measured and 88 of those where drifts θ are reported, testing continued up to failure. Failure in this study is identified with a clear change in the measured lateral force-deformation response: in monotonic loading, a noticeable drop of lateral force after the peak (at least 15% of maximum force) is interpreted as failure; and in cycling loading, failure is identified with distinct reduction of the reloading slope, and the area of the hysteresis loops and the peak force, in comparison with those of the preceding cycle(s). Such developments are typically associated with physical phenomena, such as extensive crushing or disintegration of the concrete, bar buckling, or even rupture. Typically they coincide with a drop in peak force exceeding 15% of the ultimate force.

The geometry of the test specimens in the database, the amount and layout of their reinforcement, the concrete strength, the type of steel, and the axial load cover a very broad range. For the 296 beam or column tests in which curvatures are reported, the concrete (cylindrical) strength f'_c ranges from 15 to 105 MPa, and the axial load ratio $\nu = N/A_g f'_c$ ranges from 0 to 0.95. For the 902 beam or column specimens for which deflections are reported, f'_c ranges from 15 to 120 MPa, and the axial load ratio $\nu = N/A_g f'_c$ ranges from 0 to 0.85. For the 61 wall specimens, f'_c ranges from 15 to 60 MPa, and the axial load ratio $\nu = N/A_g f'_c$ ranges from 0 to 0.9. The shear-span ratio $M/Vh = L_p/h$ ranges from 1.0 to 6.5 for prismatic specimens, and 1.75 to 5.75 for wall specimens. The ratio of diagonal reinforcement ρ_d in each diagonal direction for the 23 diagonally reinforced column specimens ranges from 0 to 1.125. The steel used in the 1012 tests can be classified in three grades: 824 tests utilized hot-rolled ductile steel with hardening ratio f_t/f_y of approximately 1.5 and strain at peak stress ϵ_{su} around 15%; 129 tests had heat-treated steel, such as the tempcore steel currently used in Europe, with f_t/f_y around 1.2 and ϵ_{su} of approximately 8%; and 59 specimens used brittle cold-worked steel with f_t/f_y of approximately 1.1 and ϵ_{su} around 4%.

DEFORMATIONS OF REINFORCED CONCRETE (RC) MEMBERS AT YIELDING

Deformations of RC members at yielding are important for the determination of their effective cracked stiffness. In earthquake-resistant design, they are also important as normalizing factors of member peak deformation demands or supplies because of their expression as ductility factors.

Curvature ϕ is convenient as a deformation measure in that it can be easily quantified in terms of section parameters and material properties on the basis of the plane-section hypothesis. If yielding of the section is signaled by yielding of the tension steel, the yield curvature is

$$\phi_y = \frac{f_y}{E_s(1 - k_y)d} \quad (1)$$

*The Appendix is available in xerographic or similar form from ACI headquarters, where it will be kept permanently on file, at a charge equal to the cost of reproduction plus handling at time of request.

whereas if it is due to significant nonlinearity of the concrete in compression beyond a level $\epsilon_c \approx 1.8f'_c/E_c$ of the extreme compression fiber strain, then

$$\phi_y = \frac{\epsilon_c}{k_y d} \approx \frac{1.8f'_c}{E_c k_y d} \quad (2)$$

The compression zone depth at yield k_y (normalized to d) is

$$k_y = (n^2 A^2 + 2nB)^{1/2} - nA \quad (3)$$

where $n = E_s/E_c$, and A and B are given by Eq. (4) or (5), if section yielding is controlled by the tension steel or by the compression zone, respectively

$$A = \rho + \rho' + \rho_v + \frac{N}{bdf_y} \quad (4)$$

$$B = \rho + \rho'\delta' + 0.5\rho_v(1 + \delta') + \frac{N}{bdf_y}$$

$$A = \rho + \rho' + \rho_v - \frac{N}{\epsilon_c E_s b d} \approx \rho + \rho' + \rho_v - \frac{N}{1.8n b d f'_c} \quad (5)$$

$$B = \rho + \rho'\delta' + 0.5\rho_v(1 + \delta')$$

In Eq. (4) and (5), ρ , ρ' , and ρ_v are the reinforcement ratios of the tension, compression, and web reinforcement (all normalized to bd) respectively; $\delta' = d'/d$, where d' is the distance of the center of the compression reinforcement from the extreme compression fibers; b is the width of the compression zone; and N is the axial load (compression: positive). In this analysis, the area of diagonal bars times the cosine of their angle with respect to the member axis is added to the reinforcement area considered in calculating ρ and ρ' .

The lower of the two values of Eq. (1) or (2) is the yield curvature. Then, the yield moment can be computed as

$$\frac{M_y}{bd^3} = \phi_y \left\{ E_c \frac{k_y^2}{2} \left(0.5(1 + \delta') - \frac{k_y}{3} \right) + \right. \quad (6)$$

$$\left. \frac{E_s}{2} \left[(1 - k_y)\rho + (k_y - \delta')\rho' + \frac{\rho_v}{6}(1 - \delta') \right] (1 - \delta') \right\}$$

The results of Eq. (1) through (5) can be compared with the experimental values of the yield curvature in 296 tests included in the database. The experimental value of curvature was obtained as the relative rotation between the section of maximum moment and a nearby section, divided by the distance of the two sections. In 124 cases, measured relative rotations include the effect of reinforcement pullout from its anchorage zone beyond the section of maximum moment, and hence, may normally lead to overestimation of the curvature. On the other hand, the effect of tension stiffening, due to concrete tensile stresses developing between discrete cracks through bond, reduces the average curvature below the value estimated from Eq. (1) or (2), neglecting tension in

Table 1—Mean, median, and coefficient of variation of ratio of experimental-to-predicted quantities at yielding

Quantity	No. of data	Mean*	Median*	Coefficient of variation, %
$\phi_{y,exp}/\phi_{y,pred,eq.(1)-(5)}$	296	1.22	1.16	32
$\phi_{y,exp}/\phi_{y,pred,Ref.12}$ —columns	121	0.84	0.83	35
$\phi_{y,exp}/\phi_{y,pred,Ref.12}$ —beams	175	1.30	1.30	25
$M_{y,exp}/M_{y,pred,eq.(6)}$	1008	1.06	1.02	20
$\theta_{y,exp}/\theta_{y,pred,eq.(7)}$	963	1.06	1.00	36
$\theta_{y,exp}/\theta_{y,pred,Ref.7}$	963	0.84	0.79	40
$\theta_{y,exp}/\theta_{y,pred,Ref.12}$	963	1.60	1.24	72
$(M_{y,exp}L_s/3\theta_{y,exp})/(M_{y,pred}L_s/3\theta_{y,pred})$	963	1.13	1.03	44
$(M_{y,exp}L_s/3\theta_{y,exp})/EI_{ACI}$	963	0.67	0.59	64
$(M_{y,exp}L_s/3\theta_{y,exp})/EI_{Ref.13}$	484 ($N \neq 0$)	1.26	1.00	82

*When coefficient of variation is high, median is more representative measure of average trend than mean, as median value of ratio of predicted-to-experimental value is always inverse of ratio of experimental-to-predicted while mean value of both ratios is higher than median.

the concrete. Finally, curvatures determined from relative rotation of two sections depend on the distance of the two sections, as this affects the number of discrete cracks and the curvature variation along this distance. Despite these inherent problems of experimental curvatures, the overall agreement of Eq. (1) through (5) with the data is fairly good and the dispersion, as expressed by the coefficient of variation of the ratio of experimental-to-predicted values, is relatively low (first row in Table 1; Fig. 1(a)). Figure 1(a) does not show any systematic increase of measured curvatures due to possible slip.

It is noteworthy that the simpler semi-empirical expressions proposed in Reference 12 ($\phi_y = 1.7f_y/E_s h$ for beams; $\phi_y = 2.12f_y/E_s h$ for rectangular columns) provide overall an equally good average fit to the same data as the fundamental Eq. (1) through (5), with only slightly higher scatter (Table 1, Rows 2 and 3).

Table 1 (fourth row) and Fig. 1(b) summarize the results of the comparison between the predictions of Eq. (1) through (6) and values of M_y measured in 1008 tests (after correction for any $P-\Delta$ effects).

Often the ratio M_y/ϕ_y is taken as the effective flexural rigidity EI of the cracked section. This ratio, however, does not reflect many important effects, such as those of inclined cracking and shear deformations along the member. Such effects refer to the member (or rather, to the shear span L_s) as a whole. They are reflected in the magnitude of the drift θ of the shear span, which, in simple or double cantilever members, is equal to the chord rotation at the member end where yielding takes place. The part of the drift or chord rotation at yield θ_y that is due to flexural deformations equals $\phi_y L_s/3$. Shear deformations and inclined cracking, as well as any fixed-end rotation due to bar pullout from the anchorage zone, add to this. Test results in the database show that, when pullout of longitudinal bars from the anchorage zone is not possible, the difference between the experimental value of θ_y and the computed value of $\phi_y L_s/3$ (attributed to inclined cracking and shear) does not have a statistically significant dependence on any of the test or specimen parameters and

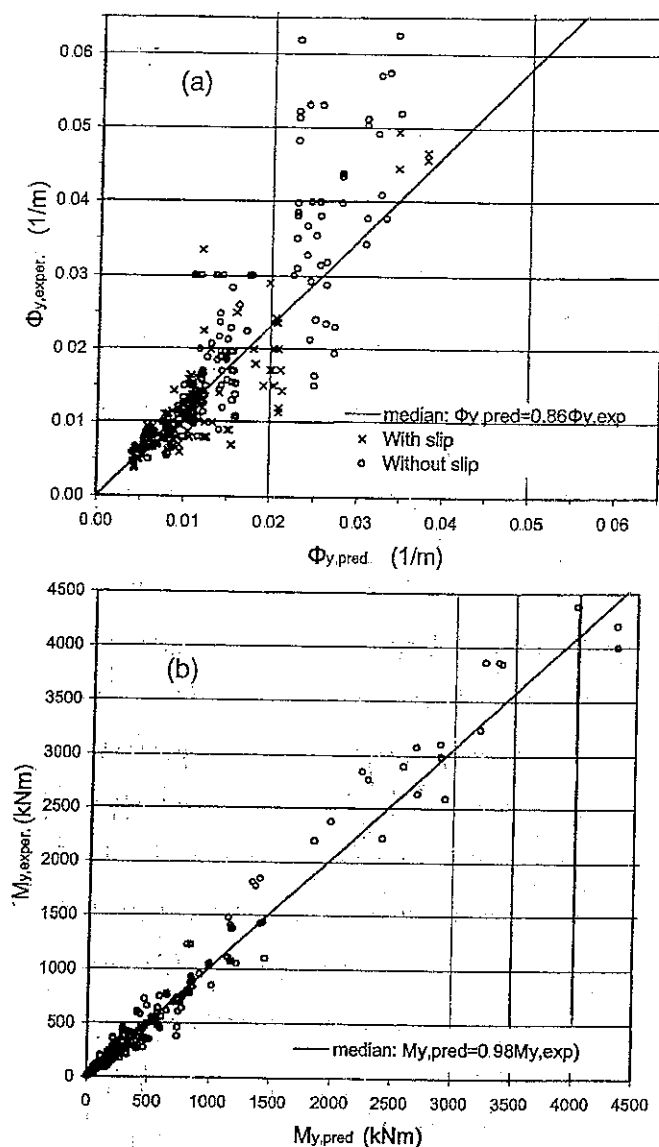


Fig. 1—Comparison of experimental and predicted values of yield: (a) curvature ϕ_y , and (b) moment M_y .

may be considered as constant. The fixed-end rotation due to bar pullout is equal to the slip from the anchorage zone at yielding of the tension steel, divided by the distance between tension and compression reinforcement $d-d'$. Slip should be proportional to the bond stress demand at yielding of the tension steel, that is, to the ratio of the bar yield force $A_s f_y$ to its perimeter πd_b (that is, to $d_b f_y$), and inversely proportional to bond strength, that is, to $\sqrt{f'_c}$. Based on this reasoning, the following relation was statistically fitted to the results of 963 tests for θ_y .

$$\theta_y = \phi_y \frac{L_s}{3} + 0.0025 + a_{sl} \frac{0.25 \epsilon_y d_b f_y}{(d-d') \sqrt{f'_c}} \quad (7)$$

The second term on the right-hand-side of Eq. (7) can be considered as the (average) shear distortion of the shear span at flexural yielding. The third term is the fixed-end rotation due to slippage; coefficient a_{sl} equals 1 if slippage of longitudinal steel from its anchorage zone beyond the end section is possible, or 0 if it is not; $\epsilon_y = f_y/E_s$ is the yield strain of

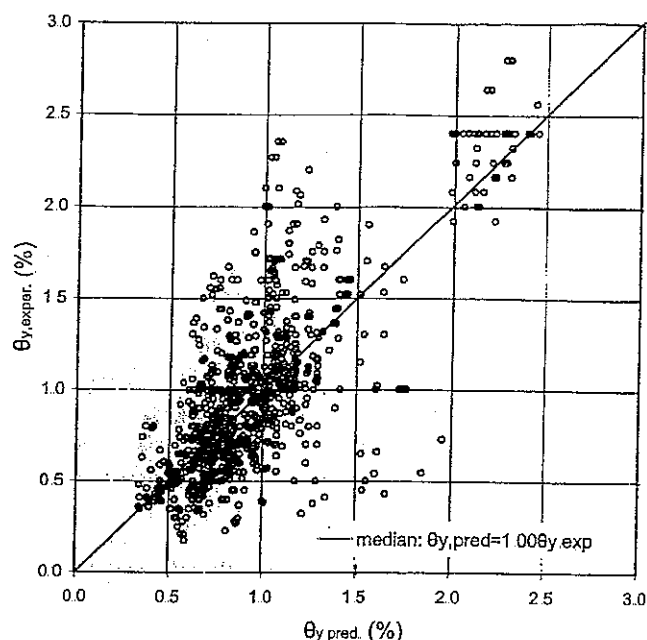


Fig. 2—Comparison of experimental and predicted values of chord rotation (or drift) at yield (963 tests).

steel; and the yield strength f_y and the concrete strength f'_c are in MPa.

Figure 2 compares the predictions of Eq. (7) with the data from which it was derived. Statistics of the ratio of the experimental to the predicted value are given at the fifth row of Table 1. On the average, Eq. (7) predicts the data well, but the dispersion is large. Overall, it does better than other models reported in the literature^{7,12} as far as agreement in the mean and the magnitude of the dispersion are concerned (Rows 5 to 7 in Table 1).

The effective rigidity of the cracked RC member to yielding EI_{ef} can be taken as $EI = M_y L_s / 3\theta_y$, with M_y and θ_y equal to the experimental values, or to those determined from Eq. (6) and (7) with the aid of Eq. (1) to (4). Experimental and calculated values of this effective rigidity are compared in the eighth row of Table 1. The effective rigidity of the cracked member to yielding is, on average, approximately 20% of that of the uncracked gross section $E_c I_g$. It is generally significantly lower than the effective rigidity given in 10.11.1 of ACI 318R-95 ($EI = 0.35 E_c I_g$ for beams or walls, $EI = 0.7 E_c I_g$ for columns) for the calculation of magnified moments in compression members and frames, or that given in 10.12.3 of ACI 318R-95 ($EI = 0.2 E_c I_g + E_s I_{se}$) for the calculation of the moment magnification in nonsway frames. This is evident from Row 9 of Table 1, which gives statistics of the ratio of the experimental effective rigidity at yielding to the value in 10.12.3 of ACI 318R-95. The proposal in Reference 13 to replace coefficient 0.2 in the ACI 318 expression with $0.27 + 0.006 L_s/h - 0.3 M/Nh$, to reproduce better moment magnification in heavily compressed slender members, is also compared in Row 10 of Table 1 with the experimental value for axially compressed specimens. Although developed in a completely different context, the Reference 13 proposal is in good average agreement with the present data and with the expression for $EI = M_{y,pred} L_s / 3\theta_{y,pred}$ fitted to them herein, albeit with considerably larger scatter than this latter expression (Rows 8 and 10 of Table 1).

Table 2—Statistics of ratio of experimental ultimate plastic (chord) rotation θ_{pl} to values suggested by FEMA 273¹ and FEMA 356^{3*}

$V/bd\sqrt{f'_c}$, units: lb. in.	$(p - p')/\rho_{bal}$	$\theta_{pl,exp.}/\theta_{pl,FEMA}$				$\theta_{u,exp.}/\theta_{u,FEMA}$				n	$\theta_{pl,exp.}/\theta_{pl,FEMA}$				$\theta_{u,exp.}/\theta_{u,FEMA}$			
		< 1.00				1.00 to 2.00					>2.00							
		m	σ	m	σ	m	σ	m	σ		m	σ	m	σ				
Beams with closely spaced stirrups [†]																		
≤ 0	0	—	—	—	—	0	—	—	—	—	0	—	—	—	—			
0 to 0.25	42	1.18	0.36	1.28	0.35	11	1.13	0.46	1.32	0.5	0	—	—	—	—			
≥ 0.25	0	—	—	—	—	0	—	—	—	—	0	—	—	—	—			
Beams without closely spaced stirrups [†]																		
$v = N/A_g f'_c$	0	—	—	—	—	0	—	—	—	—	0	—	—	—	—			
Columns with closely spaced stirrups [†]																		
≤ 0.1	76	1.43	0.78	1.48	0.70	18	1.07	0.63	1.19	0.55	5	0.78	0.17	1.03	0.13			
0.1 to 0.25	172	1.36	0.57	1.55	0.60	16	0.89	0.47	1.05	0.50	0	—	—	—	—			
0.25 to 0.4	58	1.2	0.85	1.32	0.78	5	1.12	0.52	1.24	0.43	2	0.09	0.13	0.42	0.05			
≥ 0.4	28	1.1	0.85	1.18	0.77	0	—	—	—	—	0	—	—	—	—			
Columns with no closely spaced stirrups [†]																		
≤ 0.1	44	2.75	1.33	2.59	1.14	8	2.79	1.72	2.58	1.41	5	2.01	0.54	2.18	0.40			
0.1 to 0.25	26	2.13	1.15	2.17	0.98	4	0.93	0.39	1.02	0.39	2	1.92	1.38	1.95	0.99			
0.25 to 0.4	21	1.54	1.09	1.77	0.92	1	2.57	—	2.25	—	1	2.56	—	2.25	—			
≥ 0.4	12	2.74	1.57	2.38	1.08	0	—	—	—	—	0	—	—	—	—			
$(p - p')f_y/f'_c + v$	Walls with confined boundaries [‡]																	
≤ 0.1	42	0.93	0.49	1.01	0.44	1	0.53	—	0.74	—	0	—	—	—	—			
0.1 to 0.175	8	0.65	0.26	0.69	0.19	0	—	—	—	—	0	—	—	—	—			
0.175 to 0.25	1	0.58	—	0.50	—	0	—	—	—	—	0	—	—	—	—			
≥ 0.25	0	—	—	—	—	0	—	—	—	—	0	—	—	—	—			
Walls without confined boundaries [‡]																		
≤ 0.1	1	1.28	—	1.33	—	0	—	—	—	—	0	—	—	—	—			
> 0.1	0	—	—	—	—	0	—	—	—	—	0	—	—	—	—			
Diagonally reinforced beams																		
	23	0.6	0.28	0.67	0.28	0	—	—	—	—	0	—	—	—	—			

* m = mean; σ = standard deviation; and n = number of tests.

[†] Stirrups spaced at less than $d/3$ and providing shear strength greater than $0.75V$.

[‡] Confined boundaries according to ACI 318-95

ASSESSMENT OF FEMA 273/274 and FEMA 356 ULTIMATE DRIFTS OR CHORD ROTATIONS

Recent years have seen an increased interest in the estimation of the available deformation capacity of RC members from their geometry, reinforcement, and axial and shear force levels. This interest has developed especially in relation to displacement-based seismic design and to seismic evaluation and retrofitting of existing RC structures. The "NEHRP Guidelines for the Seismic Rehabilitation of Buildings"¹⁻³ give values of the ultimate plastic hinge rotation of RC members as acceptable limiting values for primary or secondary components of the structural system under the collapse prevention earthquake, as a function of the type, reinforcement, axial and shear force levels, and detailing of RC members. These guidelines imply values of the yield rotation approximately equal to 0.005rad for RC beams and columns, or to 0.003rad for walls, to be added to plastic hinge rotations for conversion into total rotations, which are approximately equal to the chord rotation θ or drift of the shear span. Acceptable chord rotations or drifts for primary components under the collapse prevention earthquake are approximately 1.5 times lower; under the life safety earthquake, acceptable

chord rotations or drifts for the primary and secondary components are approximately 1.5 or 2 times, respectively, lower than the ultimate (chord) rotations or drifts.

The present database can be used to assess the values given for the ultimate value of the plastic rotation in the NEHRP guidelines.^{1,3} To this end, 633 flexure-controlled cyclic tests to failure were identified from the database. In these tests, the ratio of yield moment M_y to shear span L_s is less than the calculated shear strength of the specimen, even after subsequent reduction of shear strength due to cyclic inelastic flexural deformations (expressed through the displacement ductility ratio $\mu_\delta = \theta_u/\theta_y$). FEMA reports^{1,3} give values of the ultimate plastic rotation θ_{pl} (which is approximately equal to the total minus the implied yield rotation of 0.005rad in beams or columns, or of 0.003rad in walls). Thus, for the 633 cyclic tests to failure Table 2 presents separately: a) the ratio of the plastic part θ_{pl} of the experimental ultimate chord rotation (total rotation θ_u minus the experimental value of θ_y) to the ultimate plastic hinge rotation in FEMA 356³; and b) the ratio of the experimental ultimate chord rotation θ_u to the sum of the FEMA 356³ plastic rotation plus an implied yield rotation of 0.005rad for beams and columns, or of

0.003rad for walls. For beams or columns with well-detailed and closely spaced transverse reinforcement, agreement between experimental and FEMA values is good on average, albeit with significant scatter. For beams or columns with poorly detailed or widely spaced transverse reinforcement, the FEMA values are on the average well below the experimental ones. If, however, the values given in the FEMA reports^{1,3} are meant to be mean m minus one standard deviation σ bounds, then they are, on average, satisfactory for poorly detailed beams and columns, but lie on the unsafe side for well-detailed members. For walls and diagonally reinforced members for which test results are available only for well-detailed specimens, the FEMA values are on the high side, not only at the $m-\sigma$ level, but also at that of the mean. (The difference for diagonally reinforced members is partly due to the axial load on some of the test specimens, while the FEMA values^{1,3} are quoted for diagonally reinforced coupling beams.)

When the FEMA values^{1,3} and the experimental ones are compared on the basis of plastic rotations θ_{pl} , the ratio of experimental-to-FEMA values is smaller, on average, but its dispersion is higher than when the comparison is made on the basis of total ultimate rotations θ_u . As a result, if the FEMA values represent a $m-\sigma$ bound, the use of total rotations θ_u instead of plastic ones makes the FEMA values more consistent with the available data. If, on the contrary, they are meant to be average values, the use of θ_{pl} for beams and columns (but not for walls or diagonally reinforced elements) offers an advantage.

EMPIRICAL EXPRESSIONS FOR ULTIMATE CHORD ROTATION OF RC MEMBERS

The database of 875 monotonic or cyclic tests, in which θ_u values are reported and failure was controlled by flexure, is used to develop more detailed rules for the prediction of the ultimate chord rotation or drift of RC members in terms of their geometric characteristics, material properties and reinforcement, and axial and shear load levels. Two approaches are applied to this end: a) a purely empirical approach based on statistical analysis and described in this section; and b) a more fundamental approach based on curvatures and on the concept of plastic hinge length, as described in the following section.

The statistical analysis utilized data from 242 monotonic and 633 cyclic tests, all carried to flexure-controlled failure. Sixty-one tests refer to walls and the rest to beams or columns, 23 of which were diagonally reinforced. Slip of longitudinal bars from the anchorage zones beyond the section of maximum moment was possible in 703 tests, most of them cyclic.

The analysis was linear regression of the log of θ_u on the control variables or their logs without coupling between the control variables, assuming that the variance of the scatter of $\log \theta_u$ about the regression is independent of θ_u . This implies that for a given predicted value of θ_u , the coefficient of variation of the real (experimental) value is constant. In all regression analyses performed, all the parameters were initially considered as control variables, but only those that turned out to be statistically significant for the prediction of θ_u were retained. Moreover, the resulting values of the regression coefficients were rounded off.

A separate regression for 234 monotonic tests on beam and column specimens (the eight monotonic cases of walls were not enough for inclusion) gives the following expres-

sion for the ultimate chord rotation or drift θ_u in monotonic loading

$$\theta_{u, mon}(\%) = \alpha_{st, mon} \left(1 + \frac{a_{sl}}{8}\right) (0.15^v) \quad (8)$$

$$\left(\frac{\max\left(0.01, \frac{\rho' f_y'}{f_c'}\right) L_{sf_c'}}{\max\left(0.01, \frac{\rho f_y}{f_c'}\right) h} \right)^{0.425}$$

where

$L_s/h = M/Vh$ = shear-span ratio at the section of maximum moment;

ρ, ρ' = steel ratios of the tension and compression longitudinal reinforcement (not including diagonal bars); for elements with distributed reinforcement between the two flanges, the entire vertical web reinforcement is included in the tension steel;

f_y, f_y' = yield stress of tension and compression steel (for bars of different grade the sums $\Sigma \rho f_y$ or $\Sigma \rho' f_y'$ are used);

f_c' = uniaxial (cylindrical) concrete strength, MPa;

$v = N/A_g f_c'$ = axial load ratio, positive for compression;

$\alpha_{st, mon}$ = coefficient for the type of steel, equal to 1.25 for hot-rolled ductile steel, to 1.0 for heat-treated (tempcore) steel, and to 0.5 for cold-worked steel. (The 234 tests include 168 with hot-rolled steel, 32 with tempcore steel, and 34 with cold-worked steel); and

a_{sl} = coefficient for slip equal to 1 if there is slip-page of the longitudinal bars from their anchorage beyond the section of maximum moment, or to 0 if there is not (Eq. (7)).

A separate regression was performed on the 633 cyclic test data, including the 53 wall cases. The resulting expression for the ultimate chord rotation θ_u in cyclic loading is

$$\theta_{u, cyc}(\%) = \alpha_{st, cyc} \left(1 + \frac{a_{sl}}{2}\right) (1 - 0.4 a_{wall}) (0.2^v) \quad (9)$$

$$(f_c')^{0.175} \left(\frac{L_s}{h}\right)^{0.4} 1.1^{(100 \alpha \rho_{sx} \frac{f_{yh}}{f_c'})} (1.3^{100 \rho_d})$$

where

$\alpha_{st, cyc}$ = coefficient for the type of steel equal to 1.125 for hot-rolled ductile steel, 1.0 for heat-treated (tempcore) steel, and 0.8 for cold-worked steel. (The 633 tests include 542 with hot-rolled steel, 68 with tempcore steel, and 23 with cold-worked steel);

α = confinement effectiveness factor according to Reference 14, adopted also in the CEB/FIP Model Code 90¹⁰ and given by

$$\alpha = \left(1 - \frac{s_h}{2b_c}\right) \left(1 - \frac{s_h}{2h_c}\right) \left(1 - \frac{\Sigma b_i^2}{6b_c h_c}\right) \quad (10)$$

Table 3—Mean, median, and coefficient of variation of ratio of experimental-to-predicted quantities at ultimate deformation

Quantity	No. of data	Mean*	Median*	Coefficient of variation, %
$\theta_{u,exp}/\theta_{u,pred,eq.(8)}$	234	1.17	1.01	57
$\theta_{u,exp}/\theta_{u,pred,eq.(9)}$	633	1.05	1.01	41
$\theta_{u,exp}/\theta_{u,pred,eq.(11)}$	875	1.06	1.00	47
$\theta_{u,exp}/\theta_{u,pred,eq.(12)}$	875	1.08	0.99	51
$\phi_{u,exp}/\phi_{u,pred,MC90}$	261	2.77	2.15	82
$\phi_{u,exp}/\phi_{u,pred,eq.(21)}$	261	0.94	0.64	91
$\phi_{u,exp}/\phi_{u,pred,eq.(22),(23)}$	261	1.26	1.00	70
$\theta_{u,exp}/\theta_{u,pred,eq.(13)-(20),(22)-(24)}$	633	1.23	0.99	83
$\theta_{u,exp}/\theta_{u,pred,eq.(13)-(20),(22),(23),(25)}$	242	1.37	1.01	94
$\theta_{u,exp}/\theta_{u,pred,eq.(13)-(20),(22),(23),Ref.11}$	875	1.53	1.20	87

*When coefficient of variation is high, median is more representative measure of average trend than mean, as median value of ratio of predicted-to-experimental value is always inverse of ratio of experimental-to-predicted while mean value of both ratios is higher than median

with b_c , h_c denoting the width and depth of the confined core, respectively, and b_i the distances of successive longitudinal bars laterally restrained at stirrup corners or by 135 degree hooks;

$\rho_{sx} = A_{sx}/(b_w s_h) =$ ratio of transverse steel parallel to the direction x of loading;

$f_{yh} =$ yield stress of transverse steel;

$\rho_d =$ steel ratio of diagonal reinforcement in each diagonal direction; and

$a_{wall} =$ coefficient equal to 1.0 for shear walls and 0 for beams or columns.

The amounts of tension or compression longitudinal steel do not appear in Eq. (9), although they were found to be quite important for the ultimate deformation in monotonic loading (Eq. (8)). The reason is that very few of the 633 cyclic tests have unsymmetric reinforcement (even when any web steel is counted as tension reinforcement). Therefore, the (equal and opposite) effects of tension and compression reinforcement on θ_u cancel out, and their composite effect turns out as statistically insignificant.

The predictions of Eq. (8) and (9) are compared in Fig. 3(a) and (b), respectively, with the experimental data to which they were fitted. These figures show also the lines below which only 5% of the data fall. Statistics of the ratio of the experimental-to-predicted values of θ_u are given in the first two rows of Table 3. The cyclic Eq. (9) better fits the corresponding data than the monotonic Eq. (8).

The monotonic and cyclic groups of data are complementary: in the monotonic group members with unsymmetric reinforcement and the less ductile types of steel are well represented, whereas shear walls and diagonally reinforced elements are not. The situation is reversed in the group of cyclic tests. To profit from this complementary relationship and to fill any gaps of data in each one of these two groups, a regression is performed on all 875 flexure-controlled tests to failure—monotonic or cyclic—giving the following

$$\theta_u(\%) = \alpha_{st} \alpha_{cyc} \left(1 + \frac{\alpha_{sl}}{2.3}\right) \left(1 - \frac{\alpha_{wall}}{3}\right) (0.2^v) \quad (11)$$

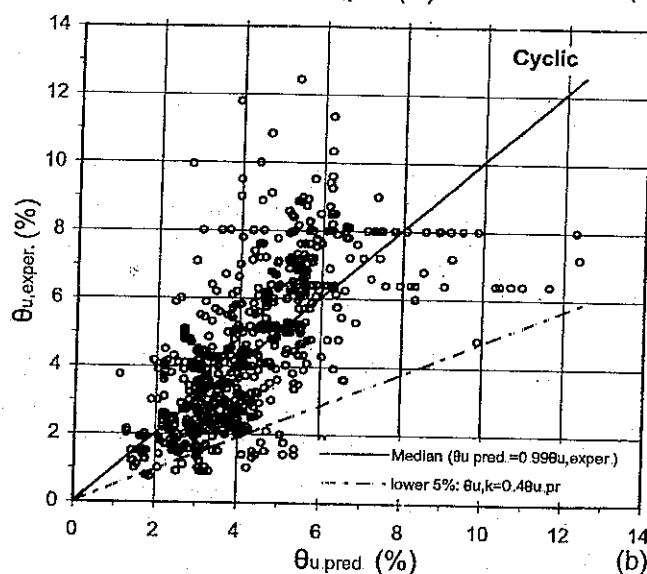
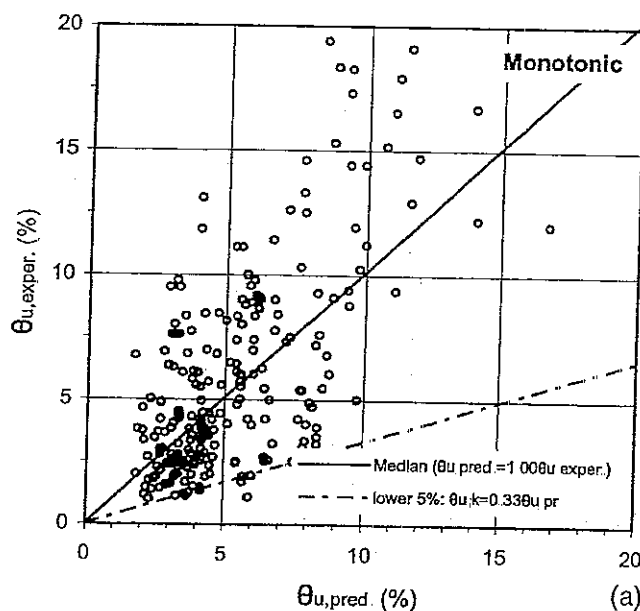


Fig. 3—Comparison of experimental ultimate chord rotations (drifts) with predictions of: (a) Eq. (8) for 234 monotonic tests on beams or columns; and (b) Eq. (9) for 633 cyclic tests.

$$\left[\frac{\max\left(0.01, \frac{\rho' f_y'}{f_c'}\right)}{\max\left(0.01, \frac{\rho f_y}{f_c'}\right)} f_c' \right]^{0.275} \left(\frac{L_s}{h} \right)^{0.45} 1.1 \left(100 \alpha_{sx} \frac{f_{yh}}{f_c'} \right) (1.3^{100 \rho_d})$$

where

$\alpha_{st} =$ coefficient for the type of steel: equal to 1.5 for hot-rolled ductile steel; 1.25 for heat-treated (tempcore) steel; and 0.8 for cold-worked steel. (The three types of steel are represented in 718, 100, and 57, respectively, of the 875 cases); and

$\alpha_{cyc} =$ coefficient equal to 1.0 for monotonic loading and to 0.6 for cyclic loading typical of load-histories applied in laboratory tests (in the 633 cyclic tests, the equivalent number of inelastic half-cycles at peak displace-

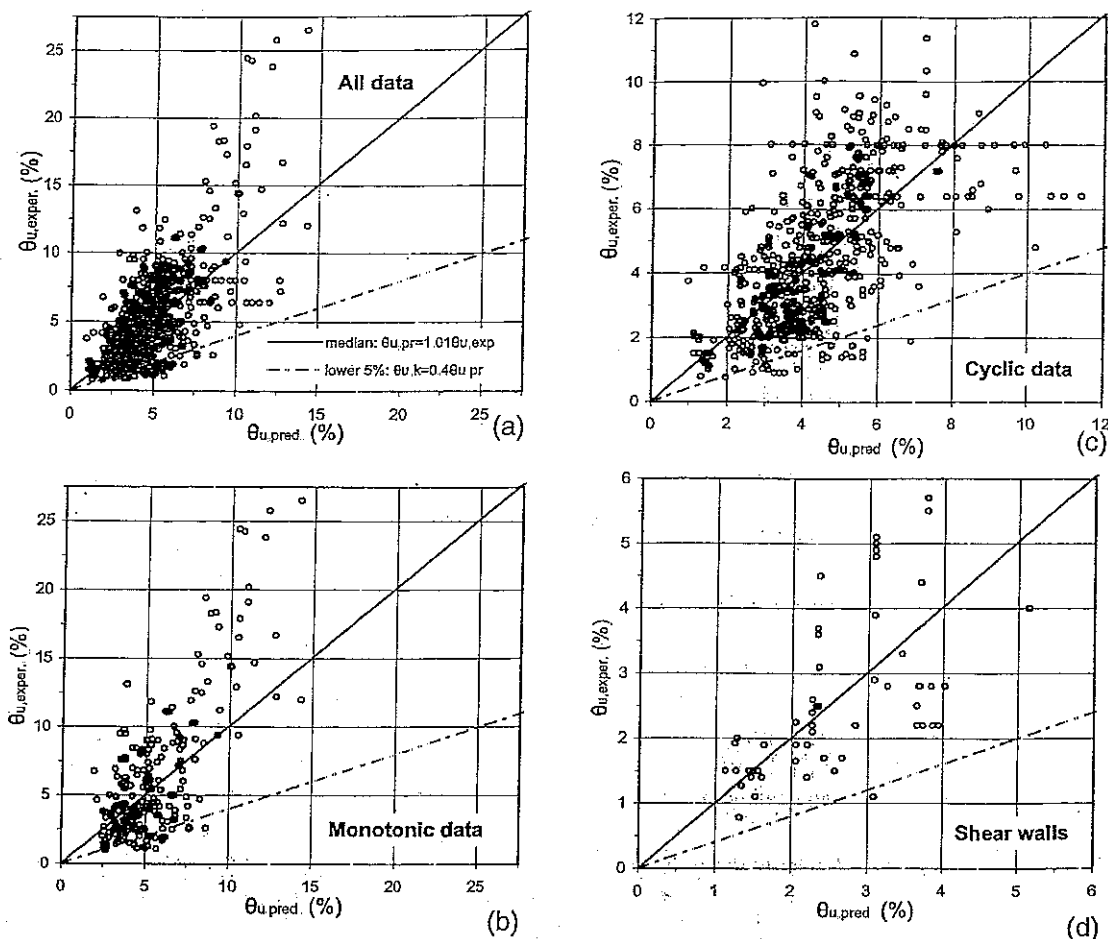


Fig. 4—Comparison of experimental ultimate chord rotations with predictions of Eq. (11) for: (a) all 875 tests; (b) 234 monotonic tests of beams or columns; (c) 633 cyclic tests; and (d) 61 shear walls

ment, $n_{eq} = \Sigma \theta_i / \theta_u$, ranges from 2 to over 50, with a mean value of 13)

To account explicitly for the effect of cycling, the equivalent number of inelastic half-cycles in each test $n_{eq} = \Sigma \theta_i / \theta_u$ was included in the regression as a control variable. This gives the following

$$\theta_{u, neq}(\%) = \alpha_{st, neq} \left(1 + \frac{a_{sl}}{3} \right) (1 - 0.35 a_{wall}) \frac{0.2^v}{n_{eq}^{0.1}} \quad (12)$$

$$\left(\frac{\max \left(0.01, \frac{\rho' f_y'}{f_c'} \right)}{\max \left(0.01, \frac{\rho f_y}{f_c'} \right)} f_c' \right)^{0.2} \left(\frac{L_s}{h} \right)^{0.475} \frac{1}{1.1} \left(\frac{100 \alpha_p f_{yh}}{f_c'} \right)^{1.1} (1.2^{100 \rho_d})$$

In Eq. (12), the steel coefficient $\alpha_{st, neq}$ takes the values 1.55, 1.35, and 0.9 for the three types of steel.

Statistics on the ratio of the experimental value of θ_u to the predictions of Eq. (11) and (12) are given in the third and fourth row, respectively, of Table 3. As suggested by the larger coefficient of variation resulting from Eq. (12), contrary to expectations, the fit to the data is slightly worse if the number of cycles is explicitly accounted for as in Eq. (12). It seems therefore that what matters for θ_u is whether or not one or more full cycles with peak displacement amplitude occur, and not the exact number of (equivalent) cycles before

that. This is better expressed by the zero-one type of variable α_{cyc} in Eq. (11) than by the equivalent number of (half) cycles in Eq. (12). Thus, Eq. (11) is selected as the best regression for the prediction of θ_u among all alternatives previously considered.

For comparison with Eq. (11), the mean and coefficient of variation of the ratio of the experimental-to-predicted value of θ_u for other well-known empirical models of θ_u of beams or columns in monotonic loading are 0.74 and 62% for the model in Reference 7, and 0.52 and 81% for Reference 8. These statistics refer to the 242 monotonic tests in the present database. For the 633 cyclic tests, they are equal to 0.71 and 223% for the model in Reference 6, and 0.58 and 62% for Reference 7. Therefore, Eq. (11) represents an advance over earlier empirical models.

From the statistical point of view, the smaller uncertainty associated with the estimation of the coefficients and exponents in the right-hand side of Eq. (11) (and expressed through their coefficients of variation) is strong evidence of its superiority over Eq. (8), (9), or (12). The values of the coefficients of variation of most of the coefficients and exponents in Eq. (11) are between 7 and 11%, except: a) those of coefficient a_{sl} for the two less ductile types of steel, which are approximately 16%; b) those of the bases in the powers of v and $100 \rho_d$, which are approximately 20%; and c) that of the base of $100 \alpha_p f_{yh} / f_c'$, which is much higher. All corresponding coefficients of variation in Eq. (8), (9), and (12) are higher, and sometimes significantly so.

Figure 4 compares the experimental values of θ_u with the predictions of Eq. (11). In Fig. 4(a), the comparison refers to all 875 data; in Fig. 4(b) and (c), the comparison refers to the 242 monotonic tests and 633 cyclic tests separately; and in Fig. 4(d), the comparison refers to the 61 monotonic or cyclic data on walls. These figures also show the median line: $\theta_{u,eq11} = \theta_{u,exp}$ of all the data and the lower characteristic line: $\theta_{u,k0.05} = 0.40\theta_{u,eq11}$, below which only 5% of the data fall. This line can be considered as a practical lower bound, for possible use in design or evaluation of RC members on the basis of displacements.

Figure 5 compares the predictions of Eq. (11) with the maximum chord rotation attained in 60 of the database cyclic tests that did not lead to failure of the specimen. All data lie below the 45 degree line, further confirming Eq. (11)

The comparisons in Fig. 4(a) to (d) suggest that there is no systematic bias of any of the groups of data (monotonic, cyclic, or walls) with respect to Eq. (11). Moreover, analyses of the scatter of the data about Eq. (11) have not revealed a lack of fit with respect to any of the independent variables (with one exception: for $L_s/h > 6$ Eq. (11) overpredicts θ_u , as the lack of inclined cracking for such values of the shear span ratio reduces overall deformations⁵). In other words, Eq. (11) scatter is uniform throughout the full range of the independent variables, including f'_c (that is, according to this analysis, θ_u increases with f'_c for values of f'_c up to 120 MPa). Nevertheless, for high values of θ_u , the predictions of Eq. (11) seem to be systematically on the low side, especially for the monotonic data. Moreover, the dispersion of the data with respect to the line expressed by Eq. (11) is large. Both these features seem to be intrinsic in the problem of prediction of deformation capacity of RC members: predictions of the monotonic plastic rotation θ_{pl} between points of inflection along the member using very sophisticated models exhibit the same features.^{5,6} In these latter models, plastic rotation was calculated by summing up contributions from discrete flexural or shear cracks, taking into account tension stiffening between them and employing very detailed models for bond-slip, for the steel postyield σ - ϵ behavior and for the concrete, confined or not. Nevertheless, in general they do not do better than Eq. (8) or (11) for scatter and bias in underpredicting high deformation capacities.

Certain aspects of the scatter about Eq. (8), (9), (11), and (12) are due to the intrinsic variability of the deformation capacity of RC members, especially under cyclic loading. To quantify this variability, 40 subgroups of practically identical cases were identified within the 875 specimens used for the development of Eq. (11). Each subgroup is comprised of two to nine specimens with practically the same parameters (even f'_c differs by less than 5%). The coefficient of variation of the value of θ_u within each subgroup ranges from 0 to 39%, with a mean value of 12.5%. This is an estimate of the contribution of natural variability to the overall coefficient of variation of 47% about the predictions of Eq. (11).

Three further points are worth mentioning regarding the variables at the right-hand side of Eq. (8), (9), (11), and (12): 1) an effort was made to include as a variable the depth h of the section separately from the shear-span ratio L_s/h instead of treating the walls separately. Despite the fact that a size-effect on the behavior of RC members is often quoted, this alternative provided much poorer predictions than Eq. (9), (11), or (12) and it was abandoned; 2) the ratio of longitudinal bar diameter d_b to stirrup spacing s_h appears as another important variable. Nevertheless, on statistical grounds, inclu-

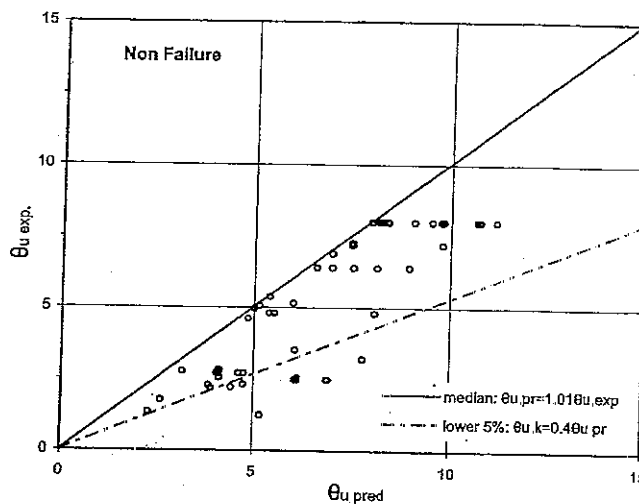


Fig. 5—Comparison of maximum chord rotation attained in 60 tests that did not reach failure, with prediction of Eq. (11) for ultimate chord rotation.

sion of d_b/s_h as a separate independent variable is not allowed, because it is strongly positively correlated with the transverse steel ratio ρ_{sx} through s_h and with the compression reinforcement ratio ρ' through d_b (cf. the strong positive correlation of ρ and ρ' in the group of cyclic tests dominated by columns). Indeed, given that ρ' is included as an independent variable, inclusion of both d_b/s_h and $\rho_{sx}f_{yh}/f'_c$ as separate, independent variables leads to the conclusion that each one of them separately has a very small influence on θ_u . Therefore it was decided to keep only the ratio of transverse steel ρ_{sx} as an independent variable, because it is more important statistically than d_b/s_h for the magnitude of θ_u . As a matter of fact, what signals the occurrence of failure in cyclic loading is not bar buckling by itself, which is delayed when the value of d_b/s_h is high, but bar fracture—possibly initiated by the curvature imposed on the bar at buckling. This curvature increases with decreasing s_h . This effect partly counterbalances the positive effect of high d_b/s_h on buckling and reduces the beneficial effect of closely spaced stirrups on θ_u ; 3) the ratio $v_o = N/(f'_c A_g + f_y A_{s,tot})$ was considered as a variable in Eq. (11) instead of $v = N/f'_c A_g$, as suggested in Reference 15. The resulting expression is almost identical to Eq. (11), except that it has 0.125^{v_o} instead of 0.2^v and that the base of the power of 100 ρ_d increases from 1.3 to 1.4. It is slightly better than Eq. (11), as far as the scatter and the coefficients of variation of the estimated coefficients and parameters are concerned, except for the coefficients of variation of the parameters referring to v_o (the 0.125) and to ρ and ρ' (exponent 0.275), which increase due to the statistical correlation introduced by the presence of ρ and ρ' in both variables. Because this alternative expression suffers from correlation between two of its independent variables (a serious flaw from the statistical point of view), it is not emphasized herein, despite the slight advantage it offers.

Equation (8), (9), and especially (11) show quantitatively how member deformation capacity is affected by the characteristics of the member and its reinforcement. More specifically, the following conclusions may be drawn:

1. Replacement of the very ductile hot-rolled steels traditionally used in seismic regions all over the world by the less ductile heat-treated tempcore steels currently dominant in Europe reduces member deformability by 15 to 20%. The

use of brittle cold-worked steel reduces member deformation capacity by half;

2. Pullout of longitudinal reinforcement from its anchorage zone beyond the member end increases member deformability, on average, by 40%. This effect is more evident in cyclic loading (Eq. (8), (9), and (11));

3. Deformation capacity is reduced by a 40% average due to full cycling at the maximum deformation. The number and magnitude of deformation cycles before ultimate seem to be unimportant;

4. Shear-span ratio seems to be the most important parameter for member deformation capacity: θ_u increases with almost the square root of L_s/h . In almost 95% of the data, the shear-span ratio is less than the threshold value of $L_s/h = 6.0$, beyond which inclined cracking does not occur, and deformation capacity may decrease with L_s/h for that reason;⁵

5. Deformability increases with approximately the fourth-root of the ratio of compression-to-tension reinforcement (the latter including the vertical reinforcement of the web of shear walls). This finding comes mainly from monotonic tests, as specimens subjected to cyclic loading typically had symmetric reinforcement;

6. The increase in deformability with confining reinforcement was found to be less than was expected, especially in monotonic loading. This was possibly due to the significant deformation capacity found in members with effectively no confinement;

7. Within the range of axial load ratio $v = N/A_g f'_c$ common in earthquake-resistant design, deformation capacity decreases approximately linearly with v , dropping by almost 50% when v increases from zero to the balance load;

8. Despite the presence of many elements with high-strength concrete in the database, the influence of concrete strength f'_c on deformation capacity was found to be as positive as that of the compression-to-tension steel ratio for values of f'_c up to 120 MPa;

9. Diagonal reinforcement has a very beneficial effect on deformation capacity: a steel ratio of 1 or 2% along each diagonal increases θ_u by 30 or 70%, respectively; and

10. All other geometric or mechanical parameters being equal, the deformation capacity of a shear wall is lower than that of a beam or column by 1/3. Statistically, this difference cannot be attributed to size effects (that is, to the larger cross-sectional depth h of walls). Physically, the difference can only partly be explained by the effects of shear, as in the walls of the database failure was either purely flexural or due to the combined effects of shear and flexure; in none of these walls was failure due to diagonal compression in the web.

ULTIMATE CURVATURE AND PLASTIC HINGE LENGTH

Ultimate drifts or chord rotations are typically expressed quantitatively on the basis of purely flexural behavior through the concepts of plastic hinge and plastic hinge length L_{pl} in which the entire inelasticity of the shear span is considered to be lumped and uniformly distributed

$$\theta_u = \phi_y \frac{L_s}{3} + (\phi_u - \phi_y) L_{pl} \left(1 - \frac{0.5 L_{pl}}{L_s} \right) \quad (13)$$

The advantages of this formulation are that: a) it represents a mechanical and physical model (that of lumped inelasticity); and b) ϕ_y , ϕ_u can be determined in terms of cross-sectional

characteristics on the basis of the plane-section hypothesis. The effects of shear, bond slip, and tension stiffening should be dealt with through L_{pl} , which is more a conventional quantity satisfying Eq. (9), rather than a physical quantity.

Under deformation-control conditions, the plastic hinge will fail either by rupture of the tension reinforcement or when the compression zone fails and sheds its load. Depending on the confinement of the compression zone by transverse reinforcement and on other parameters, these failure modes may take place either at the full section level, or at the level of the confined core after spalling of the unconfined concrete cover. For failure of the full section prior to spalling, the corresponding ultimate curvatures are:

For failure due to steel rupture at elongation equal to ϵ_{su}

$$\phi_{su} = \frac{\epsilon_{su}}{(1 - k_{su})d} \quad (14)$$

At failure of the compression zone

$$\phi_{cu} = \frac{\epsilon_{cu}}{k_{cu}d} \quad (15)$$

k_{su} and k_{cu} in Eq. (14) and (15) are, respectively, the compression zone depth at steel rupture or failure of the compression zone, both normalized to d ; and ϵ_{cu} in Eq. (15) is the extreme compression fiber strain when the compression zone fails and sheds its load. For unconfined concrete, ϵ_{cu} is approximately equal to 0.004. Assuming a stress-strain law for unconfined concrete that rises parabolically up to a strain equal to ϵ_{co} (≈ 0.002) and stays constant up to a strain of ϵ_{cu} (as is typically assumed in Europe for the calculation of the resistance of cross sections¹⁰), the plane-section assumption and equilibrium give for k_{su}

$$k_{su} = \quad (16)$$

$$\frac{(1 - \delta') \left(\frac{N}{bdf'_c} + \frac{\rho f_t}{f'_c} - \frac{\rho' f'_y}{f'_c} + \frac{\epsilon_{co}}{3\epsilon_{su}} \right) + \left(\frac{1 + \delta'}{2} \right) \frac{\rho_v (f_y + f_t)}{f'_c}}{(1 - \delta') \left(1 + \frac{\epsilon_{co}}{3\epsilon_{su}} \right) + \frac{\rho_v (f_y + f_t)}{f'_c}}$$

Steel rupture at elongation ϵ_{su} takes place prior to compression zone failure and controls the ultimate curvature if k_{su} from Eq. (12) is less than $\epsilon_{su}/(\epsilon_{cu} + \epsilon_{su})$, which is translated into the following condition for the axial load ratio

$$\frac{N}{bdf'_c} < \frac{\epsilon_{cu} - \frac{\epsilon_{co}}{3}}{\epsilon_{cu} + \epsilon_{su}} + \frac{\rho' f'_y}{f'_c} - \frac{\rho f_t}{f'_c} \quad (17)$$

$$\frac{\rho_v (f_y + f_t) \epsilon_{su} (1 + \delta') - \epsilon_{cu} (1 - \delta')}{f'_c (1 - \delta') (\epsilon_{su} + \epsilon_{cu})}$$

For values of N/bdf'_c greater than the right-hand-side of Eq. (17), spalling of the concrete cover will occur and the moment of the section will drop (at least temporarily). This will take place with yielding of the tension steel if $k < \epsilon_{cu}/(\epsilon_{cu} + \epsilon_y)$, which is translated into

$$\frac{N}{bdf'_c} \leq \frac{\rho'f'_y}{f'_c} - \frac{\rho f_y}{f'_c} - \frac{\delta'}{1-\delta'} \frac{\rho_v f_y}{f'_c} + \quad (18)$$

$$\frac{\left(\epsilon_{cu} - \frac{\epsilon_{co}}{3}\right) + (\epsilon_{cu} - \epsilon_y) \frac{\rho_v f_y}{(1-\delta')f'_c}}{\epsilon_{cu} + \epsilon_y}$$

If Eq. (18) is satisfied, k_{cu} for use in Eq. (15) is

$$k_{cu} = \frac{(1-\delta')\left(\frac{N}{bdf'_c} + \frac{\rho f_y}{f'_c} - \frac{\rho'f'_y}{f'_c}\right) + (1+\delta')\frac{\rho_v f_y}{f'_c}}{(1-\delta')\left(1 - \frac{\epsilon_{co}}{3\epsilon_{cu}}\right) + 2\frac{\rho_v f_y}{f'_c}} \quad (19)$$

(if the numerator in Eq. (19) is close to zero, ρ may be multiplied by f'_t instead of f_y). Otherwise, k_{cu} is the positive root of the following equation

$$\left[1 - \frac{\epsilon_{co}}{3\epsilon_{cu}} - \frac{\rho_v f_y}{2(1-\delta')f'_c} \frac{(\epsilon_{cu} - \epsilon_y)^2}{\epsilon_{cu}\epsilon_y}\right]k^2 + \quad (20)$$

$$\left[\frac{\rho'f'_y}{f'_c} + \frac{\rho f_y \epsilon_{cu}}{f'_c \epsilon_y} - \frac{N}{bdf'_c} + \frac{\rho_v f_y}{(1-\delta')f'_c} \left(\frac{\epsilon_{cu}}{\epsilon_y} - \delta'\right)\right]k -$$

$$\left[\frac{\rho f_y}{f'_c} + \frac{\rho_v f_y}{2(1-\delta')f'_c}\right]\frac{\epsilon_{cu}}{\epsilon_y} = 0$$

If Eq. (17) is satisfied, section failure will occur at $\phi_u = \phi_{su}$ according to Eq. (14) and (16). If it is not, attainment of ϕ_{cu} according to Eq. (15) and (18) to (20) does not necessarily signal failure. If the moment capacity of the confined section, determined on the basis of the strength f'_{cc} and ultimate strain ϵ_{cc} of confined concrete, and the dimensions b_c, d_c, d'_c of the confined core (d_c and d'_c result by subtracting from d or d' the sum of the cover and half the diameter of transverse reinforcement; b_c is obtained by subtracting double this sum) is not less than a fraction in the order of 80% of the capacity of the full but unconfined section, most of the load will be sustained by the confined core and failure will ultimately occur at the lower of the two curvature values given by Eq. (14) or (15), applied this time for the confined core (that is, dimensions b, d and d' are replaced by b_c, d_c, d'_c ; N, ρ, ρ' , and ρ_v are normalized to $b_c d_c$ instead of bd ; and f'_{cc}, ϵ_{cc} are used instead of f'_c, ϵ_{cu}).

To summarize, if Eq. (17) is satisfied, ϕ_u is determined from Eq. (14) and (15). Otherwise the moment capacities of the full but unconfined section and of the confined core after spalling of the cover are computed and compared. If the capacity of the confined core is less than 80% of that of the unconfined section, ϕ_u is the lower of: a) the value determined from Eq. (14) and (16); or b) the value determined from Eq. (15) and (18) to (20) for the confined core of the section.

This calculation of ϕ_u was applied to the 261 tests of the database for which measured values of ϕ_u are available. Three alternative confinement models were applied for this purpose: a) that of the CEB/FIP model code 1990 (MC 90),¹⁰ adopted also in Eurocode 8; b) the Mander model,⁹ as sim-

plified in Reference 11 regarding calculation of the ultimate strain ϵ_{cc} of confined concrete

$$\epsilon_{cc} = 0.004(= \epsilon_{cu}) + 1.4\epsilon_{su} \frac{\rho_s f_{yh}}{f'_{cc}} \quad (21)$$

in which ρ_s is the volumetric ratio of confining steel; and c) a model that adopts the following expression for the strength of confined concrete

$$f'_{cc} = f'_c \left(1 + 3.7 \left(\frac{0.5\alpha\rho_s f_{yh}}{f'_c}\right)^{0.87}\right) \quad (22)$$

and for ϵ_{cc} , the following modification of the Mander model

$$\epsilon_{cc} = 0.004 + 0.6\epsilon_{su} \frac{\rho_s f_{yh}}{f'_{cc}} \quad (23)$$

Coefficient α in Eq. (22) is the confinement efficiency factor, taken herein according to Eq. (10) after References 10 and 14.

Experimental values of ϕ_u are compared with the predictions of the three alternatives: a) in Table 3, through the statistics of the ratio of experimental-to-predicted values; and b) in Fig. 6, in graphic form. On the average, the MC90 confinement model underpredicts the ultimate curvature, the Mander model with the addition of Eq. (21) overpredicts it, and the model of Eq. (22) and (23) provides an unbiased fit to the data with less scatter than the others. The scatter is partly attributed to the effects of load cycling and of the fixed-end rotation due to bar pullout from the anchorage, which are not considered explicitly in the model for curvature.

Considering that the results of the comparison: a) of the predictions of Eq. (1) to (5) with the results of the tests for ϕ_y ; and b) of those of Eq. (14) to (20) and (22) and (23) with the test data for ϕ_u , constitute a verification on the average, these sets of equations are adopted for use in Eq. (13), and an appropriate expression is sought for L_{pl} . The aim is to provide a fit to the data on θ_u from the 875 tests to which Eq. (11) or (12) were fitted.

Research over all relevant element variables revealed that for Eq. (13) to apply, L_{pl} should be a function of the two variables proposed for this purpose in Reference 11: L_s and the product $d_b f_y$. If L_{pl} is taken as a linear function of these two variables, the following expressions provide the best fit to the 875 tests for which values of θ_u are available:

For cyclic loading

$$L_{pl, cy} = 0.12L_s + 0.014a_{sl}d_b f_y \quad (24)$$

For monotonic loading

$$L_{pl, mon} = 1.5L_{pl, cy} = 0.18L_s + 0.021a_{sl}d_b f_y \quad (25)$$

where f_y is in MPa, and a_{sl} is the zero-one variable used in Eq. (7) to (9), (11), and (12) for absence or presence of bar pullout from the anchorage zone beyond the section of maximum moment.

The statistics of the ratio of experimental-to-predicted value of θ_u resulting from these optimal fits are listed in Table

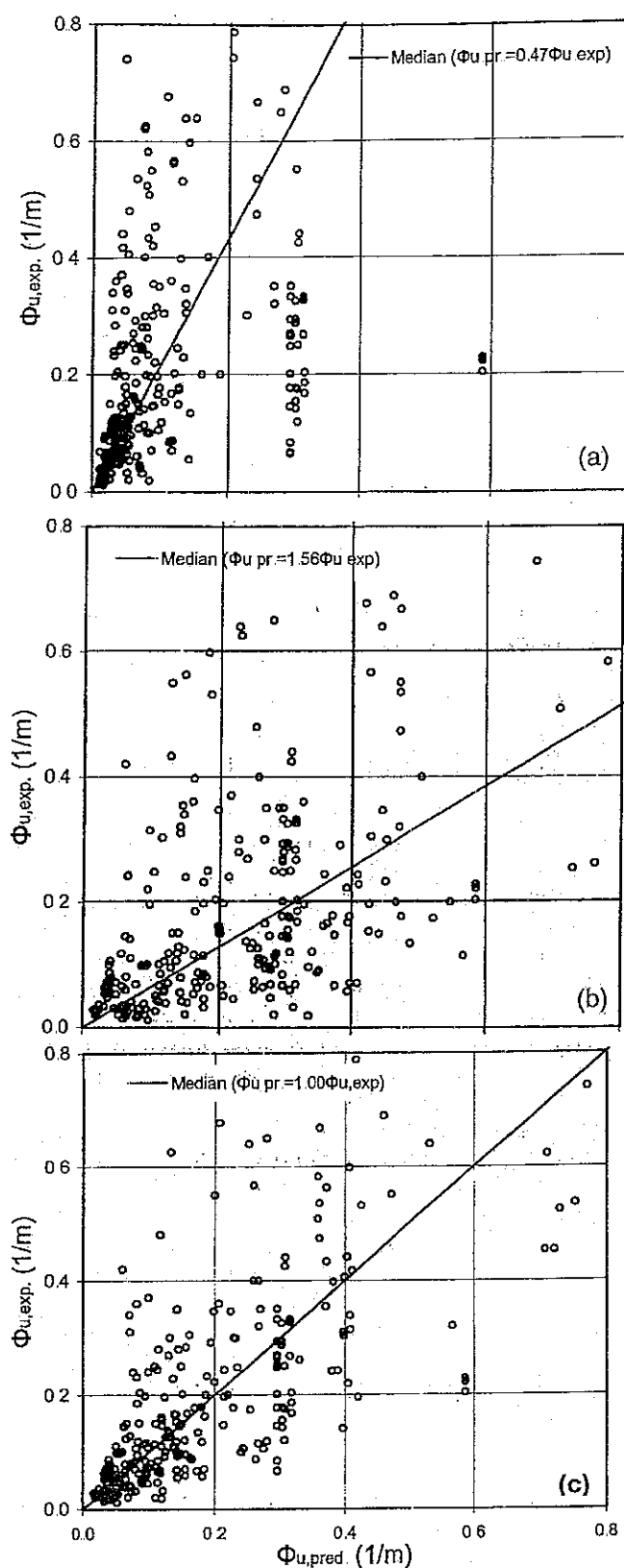


Fig. 6—Comparison of experimental ultimate curvatures with predictions from Eq. (14) to (20), for confinement models according to: (a) MC90;¹⁰ (b) Mander, Priestley, and Park⁹ and Eq. (21); and (c) Eq. (10), (22), and (23).

3, Rows 8 and 9. Figure 7 compares the predictions of Eq. (13) to (20) and (22) to (25) with the data to which they were fitted. They also show the 5% fractile lines for the data.

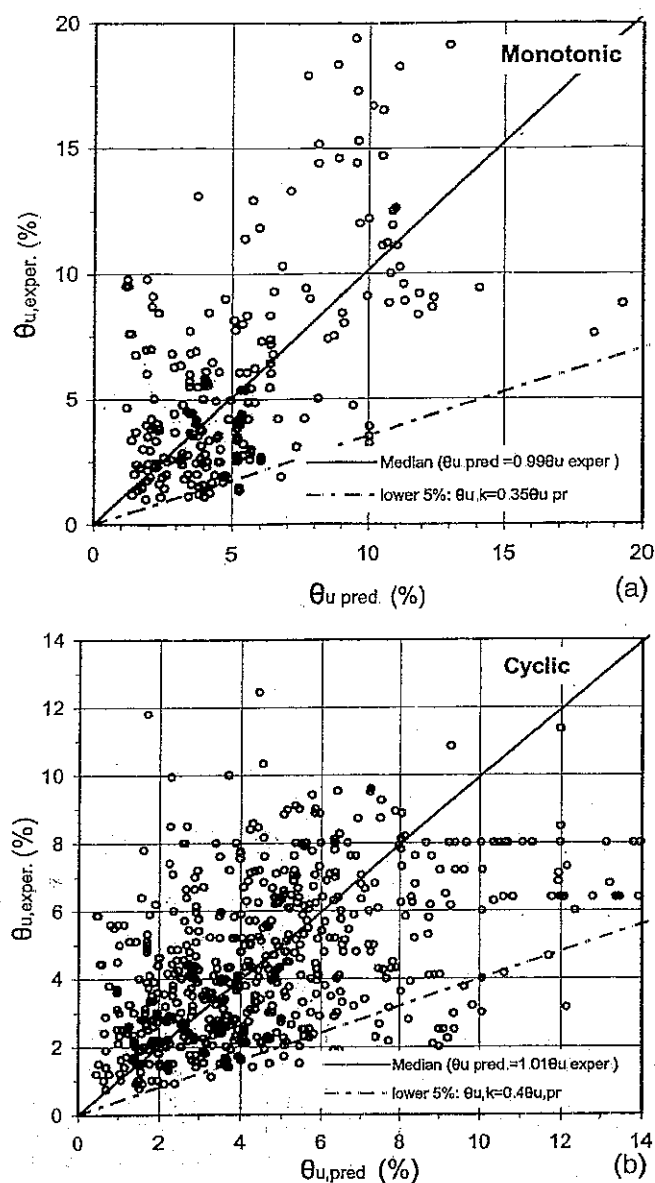


Fig. 7—Comparison of experimental ultimate chord rotations (drifts) with predictions of: (a) Eq. (13) to (20), (22), (23), and (25) for monotonic loading; and (b) Eq. (13) to (20) and (22) to (24) for cyclic loading.

Compared with Fig. 3 and 4(a) to (c), the scatter in Fig. 7 is larger. The scatter is attributed to failure of the model Eq. (13) to account properly for the effects of: a) shear and inclined cracking; and b) the type of element (wall, conventional, or diagonally reinforced beam or column). There is also considerable lack-of-fit of Eq. (13) to (20) and (22) to (25) with some of the variables, for which Eq. (11) is unbiased. It overpredicts θ_u for cold-worked brittle steels, and underpredicts it for hot-rolled ductile ones; it underpredicts θ_u for diagonally reinforced members; it overestimates the effect of confinement; and it overpredicts the value of θ_u in members with $L_v/h_v > 6$ more so than Eq. (11).

The comparison of the predictions of Eq. (13) to (20) and (22) to (24) with the maximum values of θ_u attained in 60 cyclic tests that did not reach failure, is as satisfactory as the comparison in Fig. 5.

For comparison with Eq. (13) to (20) and (22) to (24), Table 3 lists in the last row statistics of the ratio of experimental val-

ues to those predicted using the L_{pl} model in Reference 11, that is, one in which coefficients 0.12 and 0.014 in Eq. (24) are replaced with 0.08 and 0.022, respectively. These statistics are not much worse than those of Eq. (22) to (25), suggesting little sensitivity of the predictions of Eq. (13) to the details of the model for L_{pl} .

CONCLUSIONS

A large database comprised of over 1000 tests of flexure-controlled RC members in uniaxial bending with or without axial force, was assembled and used to develop simple models for the deformations of RC members at yielding and failure (ultimate). Approximately 1/4 of these tests include measurements of curvatures, which may be affected by any fixed-end rotation at the member end due to reinforcement pullout from its anchorage. Despite this and the disability of section models to capture the effects of shear or bar buckling, simple models for curvature based on first principles can reproduce on the average well the experimental curvature at yielding and ultimate. The scatter of the prediction of curvature at yielding is acceptable, but that associated with ultimate curvatures is very large.

A simple model is proposed for the chord rotation of the shear span at yielding, which comprises the familiar flexural term, a constant deformation due to shear and the contribution of any fixed-end rotation, proportional to the product of the bond stress demand and the steel yield strain. The scatter of the data about this semi-empirical model is of the same order as that of the curvature data about the model based on first principles. Its application gives effective flexural rigidities of RC members at yielding in the order of 20% of that of the uncracked gross section and in agreement with previous proposals¹³ for the flexural rigidity of heavily compressed slender columns, but with much less scatter with respect to the data.

The models proposed for yield and ultimate curvature are used to fit empirical expressions for the plastic hinge length at member ultimate deformations (Eqs. (24) and (25)). Good average fit is obtained with a plastic hinge length that is 50% greater in monotonic loading than in cyclic loading. Nevertheless, the scatter with respect to the data cannot be less than that of the model for ultimate curvature and is very high. Moreover, for certain ranges of values of the control variables, there is systematic bias of the predictions. For these reasons, alternative purely empirical models are proposed for the ultimate chord rotation. For their development, it was found necessary to combine data for monotonic and cyclic loading and for various types of elements (beams, columns, walls, and diagonally reinforced elements) into a single database, as the individual groups of elements do not include enough data to support independent fitting of empirical equations. The main outcome of this effort, Eq. (11), gives less scatter with respect to the data and is more unbiased to all the parameters than the alternatives based on rational mechanics (Eq. (13) to (20) and (22) to (25)). In this respect, it may be considered more useful for practical applications. Moreover, it shows more clearly the dependence of member deformability on the characteristics of the member and of its reinforcement. More specifically, according to Eq. (11):

1. Steel ductility is quite important for member deformability. The use of brittle cold-worked steel reduces member deformation capacity almost by 1/2, while the replacement of ductile steels traditionally used in seismic regions with

modern European tempcore steels reduces deformation capacity by 15 to 20% on the average;

2. Pullout of reinforcement from its anchorage zone beyond the member end increases deformability by approximately 40% on the average, especially under cyclic loading; in this respect it may be considered as beneficial;

3. Full cycling at the peak deformation demand reduces deformation capacity by 40% on the average, almost regardless of the previous load history;

4. Among the geometric and mechanical characteristics of the member and of its reinforcement, the shear-span ratio seems to be the most important ratio in increasing member deformation capacity. The ratio of compression-to-tension reinforcement and concrete strength f'_c rank second. The amount of confining reinforcement is less important;

5. Deformation capacity decreases almost linearly with axial load, to approximately 50% of its zero-load value at balance load; and

6. All other parameters being equal, walls have, on average, 1/3 less deformation capacity than prismatic elements.

ACKNOWLEDGMENTS

This work was sponsored by the European Commission under the IMR (Training and Mobility of Researchers) project ICONS (Innovative Seismic Design Concepts for New and Existing Structures, Contract No:ERBFM-RXCT 96-0022) and the ENVIRONMENT project NODISASTR (Novel Displacement-Based Seismic Assessment and Strengthening of RC Buildings, Contract No: ENV4-CT97-0548).

NOTATION

A	=	variable defined in Eq. (4) and (5) and used in Eq. (3)
A_g	=	gross cross-sectional area of concrete member
A_{sx}	=	area of transverse reinforcement parallel to direction of loading
a_{sl}	=	zero-one variable in Eq. (7), (9), (11), and (12), expressing effect of pullout of longitudinal bars from anchorage zone beyond section of maximum moment
a_{wall}	=	zero-one variable in Eq. (9), (11), and (12) for shear walls
B	=	variable defined in Eq. (4) and (5) and used in Eq. (3)
b	=	width of compression zone
b_c	=	width of confined core of section after spalling of concrete cover
b_i	=	distance along cross section perimeter of successive longitudinal bars laterally restrained by stirrup corner or 135 degree hook
b_w	=	width of web
d	=	effective depth of cross section
d'	=	distance of center of compression reinforcement from extreme compression fiber
d_b	=	diameter of compression longitudinal reinforcement
d_c	=	effective depth of confined core of section after spalling of concrete cover
d_c'	=	distance of center of compression reinforcement from center of stirrup (boundary of confined core)
E_c	=	elastic modulus of concrete
E_s	=	elastic modulus of steel
f'_c	=	compressive strength of unconfined concrete based on standard cylinder test
f'_{cc}	=	compressive strength of confined concrete
f_t	=	tensile strength of steel
f_y	=	yield strength of tension reinforcement
f_y'	=	yield strength of compression reinforcement
f_{yh}	=	yield strength of transverse reinforcement
h	=	depth of member cross section
h_c	=	depth of confined core of section after spalling of cover
k_{cu}	=	normalized (to d) compression zone depth at failure of compression zone
k_{su}	=	normalized (to d) compression zone depth at rupture of tension steel
k_u	=	normalized (to d) compression zone depth at section ultimate deformation
k_y	=	normalized (to d) compression zone depth at section yielding
L_{pl}	=	plastic hinge length
$L_{pl,cy}$	=	value of L_{pl} under cyclic loading, Eq. (24)

$L_{pl, mon}$ = value of L_{pl} under monotonic loading, Eq. (25)
 L_s = shear span of member ($= M/V$)
 M_y = yield moment of cross section
 N = axial force positive for compression
 n = E_s/E_c = ratio of moduli
 n_{eq} = equivalent number of inelastic half-cycles of loading at deflections equal to maximum deflection during test
 s_h = spacing of transverse reinforcement
 V = shear force
 α = confinement effectiveness factor, given by Eq. (10)
 α_{cyc} = coefficient in Eq. (8) expressing effect of cycling of loading on θ_u
 α_{st} = coefficient in Eq. (11) expressing effect of steel type on θ_u
 $\alpha_{st, cyc}$ = coefficient in Eq. (9) expressing effect of steel type on θ_u in cyclic loading
 $\alpha_{st, mon}$ = coefficient in Eq. (8) expressing effect of steel type on θ_u in monotonic loading
 $\alpha_{st, neq}$ = coefficient in Eq. (12) expressing effect of steel type on θ_u accounting for member of cycles
 δ' = d'/d
 ϵ_c = strain at extreme compression fiber beyond which yielding of cross section due to concrete nonlinearity can be identified
 ϵ_{cc} = strain where confined concrete is considered to fail in compression
 ϵ_{co} = strain at peak of concrete stress-strain diagram (~ 0.002)
 ϵ_{cu} = strain where unconfined concrete is considered to fail in compression
 ϵ_{su} = ultimate elongation of steel
 ϵ_y = steel yield strain $= f_y/E_s$
 ϕ = section curvature
 ϕ_{cu} = section curvature at ultimate failure of compression zone
 ϕ_{su} = section curvature at fracture of tension reinforcement
 ϕ_u = ultimate section curvature (at failure)
 ϕ_y = section curvature at yielding
 v = $N/A_g f'_c$ = normalized axial load ratio
 θ = drift ratio or chord rotation of shear span
 θ_{pl} = plastic rotation
 θ_u = value of θ at member failure (ultimate value)
 θ_y = value of θ at member yielding
 ρ = tension reinforcement ratio determined as ratio of tension reinforcement area to bd
 ρ' = compression reinforcement ratio determined as ratio of compression reinforcement area to bd
 ρ_d = diagonal reinforcement ratio in diagonally reinforced members, determined as ratio of area of reinforcement arranged along one diagonal to bd
 ρ_{sx} = confinement reinforcement ratio in direction of loading deter-

mined as ratio of area A_{sx} of transverse reinforcement in compression zone parallel to direction of loading to bs_h

ρ_v = web vertical reinforcement ratio of shear wall determined as ratio of total web area of longitudinal reinforcement between tension and compression steel to bd

REFERENCES

1. ATC, "NEHRP Guidelines for the Seismic Rehabilitation of Buildings," *FEMA Report 273*, Applied Technology Council for the Building Seismic Safety Council, Washington, D.C., 1997.
2. ATC, "NEHRP Commentary on the Guidelines for the Seismic Rehabilitation of Buildings," *FEMA Report 274*, Applied Technology Council for the Building Seismic Safety Council, Washington, D.C., 1997.
3. ASCE, "FEMA 356 Prestandard and Commentary for the Seismic Rehabilitation of Buildings," ASCE for the Federal Emergency Management Agency, Washington, D.C., Nov. 2000.
4. Panagiotakos, T. B., and Fardis, M. N., "Estimation of Inelastic Deformation Demands in Multistory RC Buildings," *Journal of Earthquake Engineering and Structural Dynamics*, V. 28, Feb. 1999, pp. 501-528.
5. Comité Eurointernational du Béton, "Ductility of Reinforced Concrete Structures," *Bulletin d'Information* 242, T. Telford, ed., London, May 1998.
6. Comité Eurointernational du Béton, "Ductility-Reinforcement," *Bulletin d'Information* 218, Lausanne, Aug. 1993.
7. Park, Y. J., and Ang, A. M. S., "Mechanistic Seismic Damage Model of Reinforced Concrete," *Journal of Structural Engineering*, ASCE, V. 111, No. 4, 1985, pp. 722-739.
8. Park, Y. J.; Ang, A. H.-S.; and Wen, Y. J., "Damage-Limiting Aseismic Design of Buildings," *Earthquake Spectra*, V. 3.1, 1987.
9. Mander, J. B.; Priestley, M. J. N.; and Park, R., "Theoretical Stress-Strain Model for Confined Concrete," *Journal of Structural Engineering*, ASCE, V. 114, No. 8, 1988, pp. 1827-1849.
10. Comité Eurointernational du Béton, "CEB/FIP Model Code 1990," T. Telford, ed., London, 1993.
11. Paulay, T., and Priestley, M. J. N., *Seismic Design of Reinforced Concrete and Masonry Buildings*, J. Wiley, New York, 1992.
12. Priestley, M. J. N., "Displacement-Based Approaches to Rational Limit States Design of New Structures," *Proceedings*, 11th European Conference on Earthquake Engineering, Paris, P. Bisch, P. Labbé, and A. Pecker, eds., Balkema, Rotterdam, Sept. 1998, pp. 317-335.
13. Mirza, S. A., "Flexural Stiffness of Rectangular Reinforced Concrete Columns," *ACI Structural Journal*, V. 87, No. 4, July-Aug. 1990, pp. 425-435.
14. Sheikh, S. A., and Uzumeri, S. M., "Analytical Model for Concrete Confinement in Tied Columns," *Journal of the Structural Division*, ASCE, V. 108, ST12, Dec. 1982, pp. 2703-2722.
15. Sheikh, S. A., and Khoury, S. S., "Confined Concrete Columns with Stubs," *ACI Structural Journal*, V. 90, No. 4, July-Aug. 1993, pp. 414-430.